Applied Catalysis B: Environmental 165 (2015) 700–705

Contents lists available at ScienceDirect

Applied Catalysis B: Environmental

journal homepage: www.elsevier.com/locate/apcatb

Ag/bauxite catalysts: Improved low-temperature activity and SO_2 tolerance for H_2-promoted NH_3-SCR of NO_x

Xiuyun Wang[a,b], Lilong Jiang[b], Jinyun Wang[a], Ruihu Wang[a,*]

[a] State Key Laboratory of Structural Chemistry, Fujian Institute of Research on the Structure of Matter, Chinese Academy of Sciences, Fuzhou 350002, Fujian, China

[b] National Engineering Research Center of Chemical Fertilizer Catalyst, Fuzhou University, Fuzhou 350002, Fujian, China

ARTICLE INFO

Article history:
Received 5 September 2014
Received in revised form 25 October 2014
Accepted 29 October 2014
Available online 3 November 2014

Keywords:
Ag species
Bauxite
Environmental chemistry
NO_x removal
Selective catalytic reduction

ABSTRACT

A series of Ag/bauxite catalysts were applied in H_2-promoted selective catalytic reduction (SCR) of NO_x. In comparison with $3Ag/Al_2O_3$, 3Ag/bauxite exhibits higher catalytic activity at low temperature, stronger resistance to SO_2 poisoning and better regenerability in SCR of NO_x. NO_x conversion of 3Ag/bauxite at 100–200 °C is more than 60%, which is much higher than less than 7% in $3Ag/Al_2O_3$. NH_3-TPD and *in situ* DRIFTS studies confirm the presence of Lewis and Brønsted acid sites in Ag/bauxite, and Lewis acid sites are the major acid sites. H_2-TPR, UV–vis, *in situ* DRIFTS and DFT calculation show that FeO_x and metallic Ag clusters are main active species in SCR of NO_x at low temperature.

1. Introductions

Air pollution by nitrogen oxides (NO_x) is one of the most serious environmental problems. Catalytic reduction of NO_x in exhaust gases plays an important role in NO_x abatement [1]. Several promising techniques including NO_x storage and reduction (NSR) and selective catalytic reduction (SCR) have been adopted for removal of NO_x [2]. Among these techniques, SCR of NO_x with either hydrocarbons (HC-SCR) or ammonia/urea (NH_3-SCR) is an effective process in the treatment of industrial flue gas [3]. V_2O_5/TiO_2 with WO_3 or MoO_3 as promoters are typical and efficient commercial catalysts for SCR of NO_x [4]. Nevertheless, these catalysts usually suffer from some problems, such as toxicity of vanadium, SO_2 oxidation to SO_3, over-oxidation of NH_3 to N_2O, and employment within a high and narrow temperature window of 300–400 °C [4]. Many efforts have been devoted to development of low-temperature and SO_2-tolerant SCR catalysts [5].

Recent studies have shown that Ag/Al_2O_3 is one of promising catalysts in SCR of NO_x, and shows good catalytic activity and selectivity when H_2 is co-fed with either HC or NH_3 as reductants [6,7]. Ag-based systems also possess moderate tolerance to SO_2 and H_2O, but their lack of catalytic activity below 200 °C still remains a huge problem [8]. One common way to improve low-temperature activity of Ag/Al_2O_3 is modification of Al_2O_3 support or replacement by more effective supports. For examples, Nb-doped Ag/Al_2O_3 has been found to exhibit higher NO_x conversion at low temperature than Ag/Al_2O_3 [9]. Mg-doped Ag/Al_2O_3 has been reported to possess better sulfur tolerance and higher catalytic activity than Ag/Al_2O_3 in HC-SCR of NO_x [10]. $Ag/MgO–CeO_2–Al_2O_3$ has also been reported to possess higher catalytic activity and N_2 selectivity in SCR of NO_x by ethanol than Ag/Al_2O_3 [11]. A considerable enhancement of SCR of NO_x by propene in 5 wt%$Ag/Al_2O_3–TiO_2$ has been shown in comparison with 5 wt%Ag/Al_2O_3. Similar results were also observed when Ag/Al_2O_3 was doped by Ti and Si [12]. The superior properties in these bi- or multi-oxide supports are mainly ascribed to synergetic interactions among the compositions as well as between supports and active species [5]. Since composite supports may greatly influence catalytic performances of SCR catalysts, the exploration of new types of supports has attracted considerable attention in SCR of NO_x. In the context, bauxite is well known to be a cheap, readily available and non-toxic oxide support in the catalytic reactions, which is composed of Al_2O_3, FeO_x, SiO_2, TiO_2, CaO and trace of platinum [13], the compositions are advantageous in NO_x removal [13,14], but the investigation of Ag/bauxite in SCR of NO_x is still unexplored. In our continuous efforts to develop low-temperature and SO_2-tolerant SCR catalysts, herein, we present a series of Ag/bauxite catalysts for SCR of NO_x, NO_x conversion in Ag/bauxite is much higher than Ag/Al_2O_3 at 100–250 °C, moreover,

* Corresponding author. Tel.: +86 591 83711028; fax: +86 591 83714946.
E-mail address: ruihu@fjirsm.ac.cn (R. Wang).

http://dx.doi.org/10.1016/j.apcatb.2014.10.080
0926-3373/

3Ag/bauxite shows better sulfur resistance and regeneration ability than 3Ag/Al_2O_3 in H_2-promoted NH_3-SCR of NO_x.

2. Experimental

2.1. Catalyst preparations

Ag/bauxite was prepared by deposition method. Thermal-treatment natural bauxite (1.0 g) in water (50 mL) was heated to 60 °C for 3 h, $AgNO_3$ (1, 3 and 6 wt% Ag against bauxite) in H_2O (10 mL) were dropwisely added, the resultant mixture was evaporated to dryness at 60 °C, dried at 120 °C overnight and calcined at 550 °C for 2 h. For comparison, 3 wt% Ag was also deposited on commercial γ-Al_2O_3 (Alfa-Aesar, 180 m^2/g) with the same method as that of Ag/bauxite.

2.2. Catalytic activity tests

SCR activity measurement was performed in a fixed-bed stainless steel reactor (inner diameter = 8 mm). Before each test, a sample of 0.5 g was reduced by 5 vol% H_2/Ar at 500 °C for 2 h, and followed by treatment using 3 vol% O_2/Ar at 500 °C for 2 h. After cooled to test temperature, the feed gas (482 ppm NO, 500 ppm NH_3, 0.67 vol% H_2 and 3 vol% O_2 balanced with Ar) was introduced using mass-flow controllers at a total flow rate of 600 mL/min, and the corresponding GHSV is 72,000 h^{-1}. 10.0 vol% H_2O was added to feed gas stream to examine resistance of catalysts against H_2O at 350 °C. SO_2 poisoning experiment was performed by exposing samples to the feed gas containing additional 50 ppm SO_2 at 350 °C. The sulfated samples were regenerated by 3.5 vol% H_2 at 500 °C for 60 min. The selectivities of N_2 and N_2O were analyzed using a GC7820 A. Transient response method (TRM) of 3Ag/bauxite was carried out at 200 °C [14b]. 500 ppm NO, 0.05 vol% O_2, 1 vol% H_2 and 500 ppm NH_3 were fed. The outlet gas concentrations were continuously monitored by mass spectrometer and UV analyzer.

2.3. Characterizations

X-ray diffraction (XRD) patterns were recorded on a RIGAKU-Miniflex II X-ray diffractometer with Cu K_α radiation (λ = 1.5406 Å). N_2 physisorption measurement was performed on an ASAP 2020 apparatus, the sample was degassed in vacuo at 180 °C at least 6 h before the measurement. Transmission Electron Microscope (TEM) was performed on a FEI TECNAI G^2F20 microscope. O_2 chemisorption at 150 °C was conducted on an AutoChem 2920 equipped with a TCD detector. Before O_2 chemisorption measurement, the calcined sample was reduced *in situ* by 20 vol% H_2/Ar (50 mL/min) at 400 °C for 3 h, and then outgassed under vacuum at 350°C for 16 h.

Diffuse reflectance UV–vis spectra were collected on a Perkin Elmer Lambda 950 spectrophotometer equipped with an integrating sphere in the range from 200 and 800 nm using $BaSO_4$ as the reference for baseline emendation. To keep Ag state as it was, the sample was quickly cooled to room temperature under N_2 after SCR test.

Ammonia temperature-programmed desorption (NH_3-TPD) was conducted on an AutoChem 2920 equipped with a TCD detector. A sample of 0.1 g was pretreated in Ar at 500 °C for 1 h. After cooled to 50 °C, the sample was exposed to 1 vol% NH_3/Ar for 0.5 h, followed by flushing with Ar at 100 °C to remove physisorbed ammonia, and then cooled down to 50 °C. NH_3-TPD was measured from 50 to 800 °C at 10 °C/min.

In situ diffuse reflection infrared Fourier transform spectroscopy (DRIFTS) was recorded on a Nicolet Nexus FT-IR spectrometer in the range of 650–4000 cm^{-1} with 32 scans at a resolution of 4 cm^{-1}. Prior to each experiment, the sample was pretreated at 350 °C for 0.5 h in a gas flow of N_2 to remove any adsorbed impurities, and then cooled down to 50 °C. The background spectrum was collected under N_2 and automatically subtracted from the sample spectra. Afterward, NH_3 (500 ppm balanced with He) was introduced to the cell in a flow rate of 30 mL/min at 100 °C for 1 h to ensure complete absorption saturation. After physisorbed ammonia was removed by flushing wafer with helium at 100 °C for 3 h, DRIFTS spectra were recorded at 50–400 °C.

H_2 temperature-programmed reduction (H_2-TPR) was performed on AutoChem II 2920 equipped with a TCD detector, in which the samples were pretreated in an air flow (30 mL/min) at 500 °C for 0.5 h, and were followed by purging with Ar (30 mL/min) at the same temperature for 0.5 h, after cooled to room temperature, the temperature was increased at 5 °C/min up to 800 °C by a temperature-programmed controller in gas flow of 10 vol% H_2/Ar (30 mL/min).

Density functional theory (DFT) calculations were carried out using Gaussian 03 (Revision D.02) suite of programs. Geometric optimization of the structures and frequency analyses were carried out by using MP2 (Second order approximation of Møller-Plesset perturbation theory) method. In these calculations, the Hay-Wadt double-ζ with a Los Alamos relativistic effect basis set (Lanl2dz) consisting of the effective core potentials (ECP) was used to describe all of atoms. The analytically calculated vibrational wavenumbers were scaled by 0.963. The theoretical IR spectra were simulated by GaussSum 2.2.5 program. The spectra were convoluted with Lorentizian curves, and the full width at half maximum of each peak was 3 cm^{-1}.

3. Results and discussion

3.1. Texture and structure properties

BET surface area of bauxite is 194 m^2/g, which is decreased to 158–192 m^2/g after the addition of Ag (Table S1) owing to blockage or filling of partial pores by Ag species. Similarly, the addition of 3 wt% Ag to γ-Al_2O_3 results in the decrement of surface area from 180 to 137 m^2/g. Pore diameters in Ag/bauxite are in the mesoporous range from 2.21 to 2.56 nm, which are much smaller than that in 3Ag/Al_2O_3. XRD patterns demonstrate that both bauxite and Ag/bauxite possess three strong characteristic peaks (Fig. S1), which are identified as Al_2O_3 (JCPDS No. 10-425), Fe_2O_3 (JCPDS No. 06-0502) and mullite phase. In addition, a weak peak at 14.4° is also observed in Ag/bauxite, which is assigned to the characteristic peak of beidellite [$Al_{13}Si_{19}Al_5O_{60}(OH)_{12}Na_2$] phase. No characteristic peaks of Ag species are observed in Ag/bauxite and 3Ag/Al_2O_3, suggesting that they are finely dispersed on bauxite (Al_2O_3) or they are too small to be detected by XRD analysis. TEM images show that the average size of Ag particles in 3Ag/bauxite is 4.5 nm, which is much smaller than that in 3Ag/Al_2O_3 (7.5 nm) (Fig. S2). O_2 chemisorption was further performed to investigate dispersion of Ag. As shown in Table S1, Ag dispersion in 3Ag/bauxite is 24%, which is higher than 3Ag/Al_2O_3 (16%). The mean diameters of Ag particles are also derived from dispersion values assuming the particles to be rough sphere in shape, Ag particle sizes in 3Ag/bauxite and 3Ag/Al_2O_3 are 5.8 and 7.4 nm, respectively.

3.2. UV–vis spectra

Since various types of Ag species have been proposed as the active components in reduction of NO_x and partial oxidation of NH_3, diffuse reflectance UV–vis study was used to identify the states of Ag [14]. As shown in Fig. 1, there are three absorption bands in Ag/bauxite, representing three different states of Ag. Peaks at 219 nm may be assigned to the electronic transition of highly dispersed ionic Ag^+ from $4d^{10}$ to $4d^95s^1$ [15], while bands at 320 and

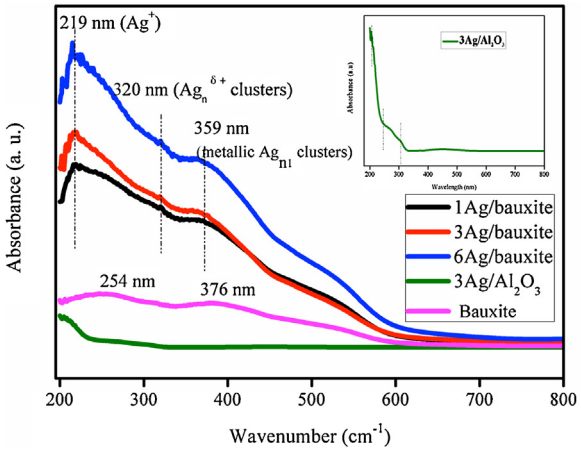

Fig. 1. UV–vis spectra of bauxite, Ag/bauxite and $3Ag/Al_2O_3$.

359 nm are attributed to $Ag_n^{\delta+}$ clusters and Ag_n^0 clusters, respectively [3]. Intensities of Ag^+ and Ag_n^0 bands in Ag/bauxite are higher than that in $3Ag/Al_2O_3$, and are in the following sequence: 6Ag/bauxite > 3Ag/bauxite > 1Ag/bauxite. It should be mentioned that there are two weak absorption bands in bauxite, the band at 254 nm may be assigned to the co-existence of Fe^{3+} sites in octahedral coordination and Ti atoms in pentahedral or octahedral coordination environment [2d,3d], while the band at 376 nm corresponds to small Fe_2O_3 clusters. The two weak bands are covered by Ag species in Ag/bauxite.

3.3. SCR activity test

The catalytic activities of Ag/bauxite and $3Ag/Al_2O_3$ in SCR of NO_x are shown in Fig. 2. Bauxite itself possesses catalytic activity in SCR of NO_x. NO_x conversion is over 40% at 100–250 °C, which is higher than that of $3Ag/Al_2O_3$. It is well known that Fe species may serve as active components in SCR of NO_x at low temperature [4]. Thus, the catalytic activity in bauxite probably results from the presence of FeO_x. The addition of Ag into bauxite results in significant promotion of NO_x conversion. NO_x conversions at 100 °C in 1Ag/bauxite, 3Ag/bauxite and 6Ag/bauxite are 42, 60 and 61% (Fig. 2), respectively, which are risen to 50, 63 and 82% at 200 °C, respectively. Obviously, NO_x conversion of Ag/bauxite is gradually enhanced when Ag content is increased from 1 to 6 wt% at 100–250 °C, the presence of Ag_n^0 clusters is probably responsible for the increment of catalytic activity at low temperature [6b]. In 3Ag/bauxite and 6Ag/bauxite, NO_x conversions increase as the temperatures are elevated, and reach the maximum at 350 and 250 °C, respectively. Subsequent drop of conversion is observed above 250 °C in 6Ag/bauxite, which is attributed to the presence of more Ag^+ species in 6Ag/bauxite, resulting in faster oxidation of NH_3 than NO at high temperature. It should be mentioned that NO_x conversion of 3Ag/bauxite is higher than that of 6Ag/bauxite above 300 °C. For instance, NO_x conversions at 350 °C in 3Ag/bauxite and 6Ag/bauxite are 99 and 81%, respectively. $3Ag/Al_2O_3$ shows much low activity at 100–200 °C (<10%), which is consistent with literature report of 7% conversion at 200 °C in Ag/Al_2O_3 [7]. Above 250 °C, NO_x conversion begins to quickly increase with a maximum of 99% at 350 °C, which is close to that in 3Ag/bauxite. The light-off temperature T_{50} (the temperature where NO_x conversion reaches 50%,) is as high as 300 °C in $3Ag/Al_2O_3$, while it is less than 100 °C in 3Ag/bauxite. Ag/bauxite possesses higher low-temperature SCR activity than Ag/Al_2O_3, which may be ascribed to the presence of FeO_x species in bauxite and the increment of metallic Ag_n^0 clusters. N_2 selectivity of 3Ag/bauxite was also investigated, which is more than 90% in 100–400 °C (Fig. S3a). TRM experiment of 3Ag/bauxite shows the formation of N_2O is 13 ppm at 200 °C (Fig. 3b). It is noteworthy that both 3Ag/bauxite and $3Ag/Al_2O_3$ possess low SCR activity in the absence of H_2 (Fig. S4), but 3Ag/bauxite exhibits higher SCR activity than $3Ag/Al_2O_3$ at 100–400 °C owing to the presence of FeO_x in bauxite [4]. These results indicate H_2 plays an important role in SCR of NO_x.

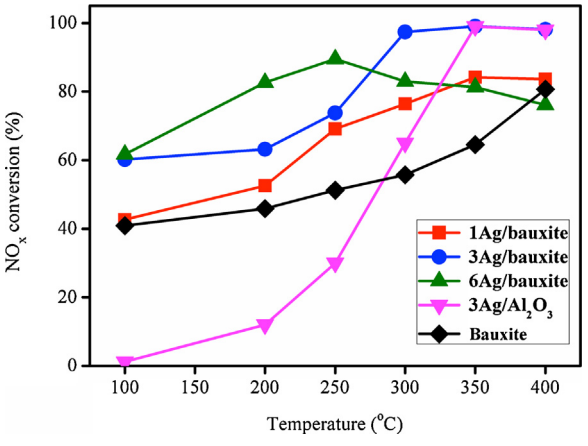

Fig. 2. NO_x conversion for bauxite, Ag/bauxite and $3Ag/Al_2O_3$.

The simultaneous existence of SO_2 and H_2O in exhaust gases is known as a deactivation cause of SCR catalysts at low temperature due to the formation of NH_4HSO_4 [3]. The improvement of SO_2 and H_2O tolerance is one of challenges for NH_3-SCR catalysts. SO_2-tolerance and regenerability of 3Ag/bauxite and $3Ag/Al_2O_3$ were initially examined at 350 °C owing to similarity of their NO_x conversion at the temperature. As shown in Fig. 3a, their NO_x conversion at 350 °C maintains 99% after lasting for 20 h. However, the presence of 50 ppm SO_2 results in quick detriment of NO_x conversion from 99% to 47% in $3Ag/Al_2O_3$. Interestingly, NO_x conversion in 3Ag/bauxite is just lowered to 73% under the same conditions. The superior tolerance toward SO_2 is ascribed to the presence of FeO_x and TiO_2 in bauxite, which can inhibit the formation of sulfates and/or sulfites. After the supply of SO_2 was cut off and sulfated catalysts were regenerated by 3.5 vol% H_2 at 500 °C, NO_x conversions of 3Ag/bauxite and $3Ag/Al_2O_3$ rapidly return to 96% and 83%, respectively. These results demonstrate that $3Ag/Al_2O_3$ also possesses good regeneration ability, and 3Ag/bauxite is more sulfur-resistant. 3Ag/bauxite was also tested in a feed gas stream containing 10 vol% H_2O at 350 °C. As shown in Fig. 3b, NO_x conversion decreases from 99 to 68% after H_2O was introduced into the catalytic system. After cutting off the supply of H_2O, NO_x conversion is restored to 98%. When 10 vol% H_2O and 50 ppm SO_2 are simultaneously introduced to feed gas, NO_x conversion of 3Ag/bauxite is lowered to 60%, and NO_x conversion is restored to above 90% after removal of SO_2 and H_2O from the feed gas.

3.4. H_2-TPR

In order to disclose correlation between SCR performances and redox properties of the catalysts, the results of H_2-TPR are presented in Fig. 4. Bauxite shows two broad reduction peaks similar to Fe_2O_3. The peak at 420 °C corresponds to the reduction of Fe_2O_3 to Fe_3O_4, and the other peak at 683 °C is assigned as the reduction of Fe_3O_4 to FeO and subsequent reduction to Fe. In Ag/bauxite, the two reduction peaks shift to lower temperatures, suggesting the presence of synergetic effect between bauxite and Ag. In addition, one additional weak peak below 100 °C is observed in Ag/bauxite, corresponding to one-step reduction from Ag^+ to $Ag_n^{\delta+}$ regardless of Ag contents [13]. These results further suggest that AgO_x and FeO_x are main active components of NO_x reduction in Ag/bauxite.

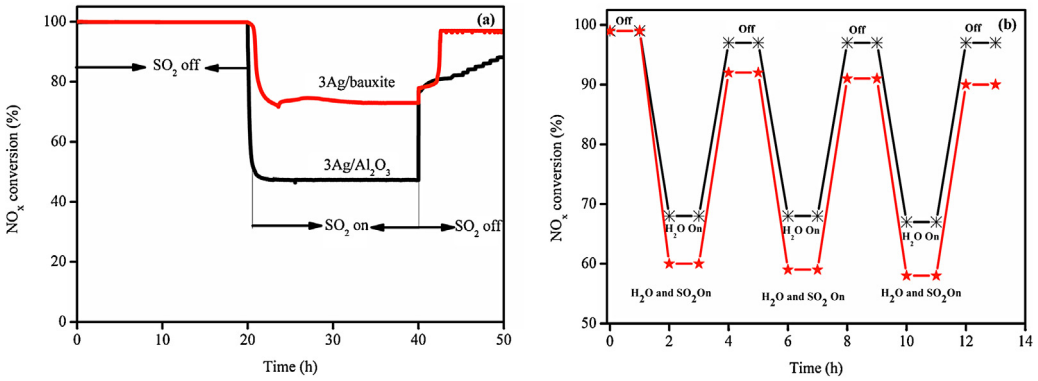

Fig. 3. (a) Stability test, SO_2 poisoning and regeneration of 3Ag/bauxite and $3Ag/Al_2O_3$ at 350 °C; (b) Effect of H_2O, $H_2O + SO_2$ on NO_x conversion of 3Ag/bauxite at 350 °C.

However, two weak reduction peaks at 389 and 622 °C are observed in $3Ag/Al_2O_3$, which are assigned to the reduction of Ag^+ to metallic Ag and the reduction of atomic oxygen [4c], respectively. It was reported that Ag^+ can be reduced into $Ag_n^{\delta+}$ cluster at low temperature, while Ag^+ is usually reduced into metallic Ag at high temperature [3c,4c], resulting in the different reduction temperatures of Ag species in 3Ag/bauxite and $3Ag/Al_2O_3$. It should be mentioned that the reduction peak of Ag^+ to metallic Ag is overlapped by the reduction of Fe_2O_3 to Fe_3O_4. Moreover, the peak area in Ag/bauxite is much higher than that in Ag/Al_2O_3, implying higher reduction ability of Ag/bauxite, which is responsible for superior low-temperature SCR activity.

3.5. NH_3-TPD

The adsorption and activation of NH_3 on the active sites of catalyst surface have important effects on NH_3-SCR of NO_x [15], NH_3-TPD was performed to investigate surface acid amount and acid strength of Ag/bauxite and $3Ag/Al_2O_3$. As shown in Fig. 5, NH_3 desorption profiles present two distinct desorption peaks, indicating that there are two kinds of acid sites on the surface of the catalysts. The peak at low temperature with a shoulder peak (<400 °C) can be assigned to NH_3 desorption from weak and medium NH_4^+ acid sites, which bind with the surface hydroxyl group. The corresponding NH_3 desorption values in 1Ag/bauxite, 3Ag/bauxite and 6Ag/bauxite are approximately 1.52, 2.68 and 2.99 mmol/g, respectively (Table S1), which are apparently higher than that in $3Ag/Al_2O_3$ (0.97 mmol/g), suggesting that bauxite can greatly increase the amount of Brønsted acid site in Ag/bauxite. Moreover, the peak at 101 °C in $3Ag/Al_2O_3$ is shifted to 112 °C in 3Ag/bauxite and 6Ag/bauxite, suggesting that the strength of Brønsted acid sites is slightly intensified. The other NH_3-TPD peak at high temperature (>500 °C) is related to desorption of NH_3 bounding to Lewis acid sites [16]. The bands in 1Ag/bauxite, 3Ag/bauxite, 6Ag/bauxite and $3Ag/Al_2O_3$ are centered at 575, 592, 610 and 613 °C, respectively. The corresponding area of desorption peak follows the order: $3Ag/Al_2O_3$ < 1Ag/bauxite < 3Ag/bauxite < 6Ag/bauxite. Since the area of desorption peak is proportional to acid amount, Ag/bauxite presents much more Lewis and Brønsted acid sites than $3Ag/Al_2O_3$, which facilitates adsorption and activation of NH_3 in SCR of NO_x, resulting in remarkable improvement of low-temperature catalytic activity in NO_x removal.

3.6. *In situ* DRIFTS

In situ DRIFTS were investigated to better understand the nature of acid sites in 3Ag/bauxite and $3Ag/Al_2O_3$. For 3Ag/bauxite (Fig. 6a), the bands at 1026, 1142 and 1230 cm^{-1} may be assigned to symmetric bending vibrations of the coordinated NH_3 on Lewis acid sites, while the band at 1582 cm^{-1} corresponds to anti-symmetric bending vibration [17]. The bands at 1468 and 1737 cm^{-1} are attributed to —NH_2 vibration and symmetric bending vibrations of NH_4^+ ions on Brønsted acid sites, respectively [17]. Obviously, the intensity of the peaks decreases with increment of temperature in 3Ag/bauxite, indicating that adsorbed NH_3 is unstable at high temperature. The band at 1350 cm^{-1} can be assigned to the coordinated NH_3 on Lewis acid sites, which is also observed at 1333 cm^{-1} in Ag/Al_2O_3 (Fig. 6b). The other two bands at 1463 and 1408 cm^{-1} in Ag/Al_2O_3 may be assigned to —NH_2 vibration

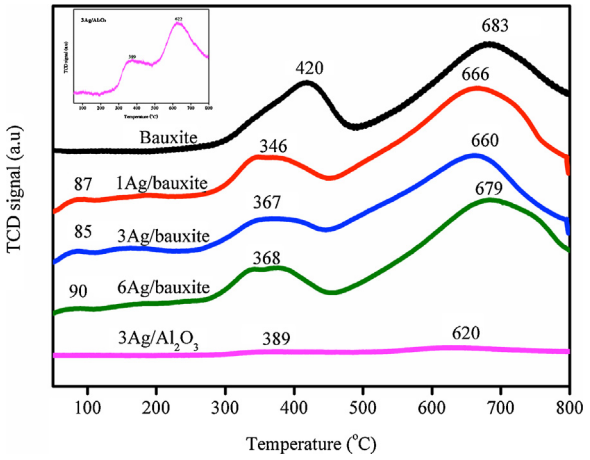

Fig. 4. H_2-TPR profiles of bauxite, Ag/bauxite and $3Ag/Al_2O_3$.

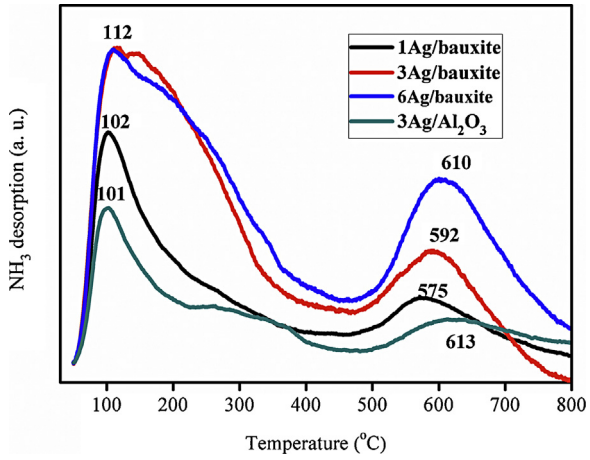

Fig. 5. NH_3-TPD profiles of Ag/bauxite and $3Ag/Al_2O_3$.

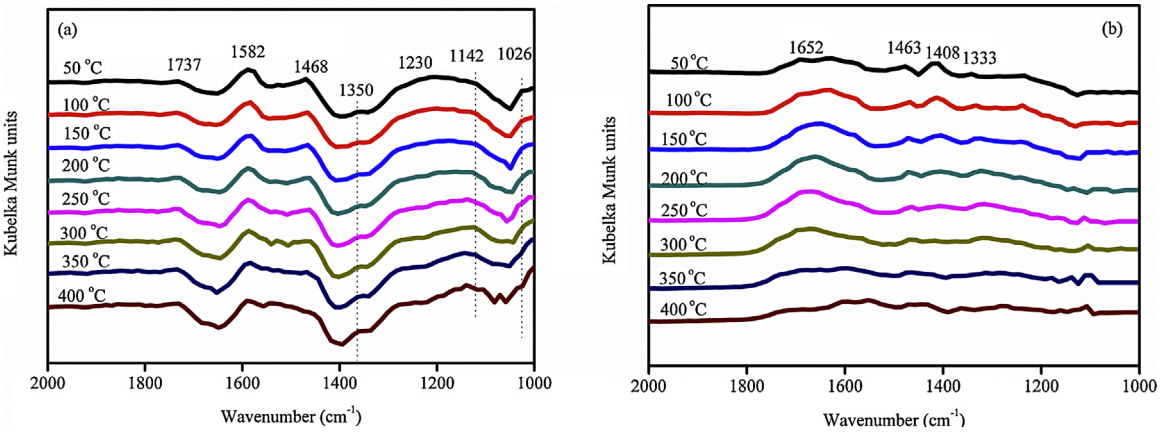

Fig. 6. *In situ* DRIFTS of NH_3 adsorption at different temperatures for (a) 3Ag/bauxite and (b) $3Ag/Al_2O_3$.

and anti-symmetric bending vibration of NH_4^+ ions on Brønsted acid sites, respectively, while the peak at 1652 cm^{-1} is related to symmetric bending vibration of NH_4^+on Brønsted acid site [17].

The amounts of Lewis and Brønsted acid in Ag/bauxite and Ag/Al_2O_3 were calculated from their respective *in situ* DRIFTS based on literature methods [5c,16]. As shown in Fig. S5, the amounts of Brønsted acid and Lewis acid in Ag/bauxite obviously decrease as temperature increases. However, the amount of Brønsted acid in Ag/Al_2O_3 slowly increases with increment of temperature and reaches the maximum at 250 °C, and then quickly drops. Obviously, the amount of Lewis acid in Ag/bauxite is more than that in Ag/Al_2O_3 in the range of test temperatures (50–400 °C), while Brønsted acid in Ag/bauxite is less than that in Ag/Al_2O_3 at 200–300 °C. For instance, the amounts of Lewis acid sites at 200 °C in Ag/bauxite and Ag/Al_2O_3 are 39.7 and 3.0, respectively, while the values of Brønsted acid sites at 200 °C in Ag/bauxite and Ag/Al_2O_3 are 3.6 and 3.8, respectively. These results indicate that Lewis acid is the major acid sites in Ag/bauxite, which is responsible for high catalytic activity at low temperature.

3.7. DFT calculation

DFT atomistic modeling is applied to investigate NH_3 adsorbed on surface of Ag/bauxite, which are possible intermediates that participate in the catalytic cycles. The simulated FTIR spectrum of the surface NH_3 and NH_4^+ species bonded with main compositions of Ag/bauxite is shown in Fig. 7 and Fig. S6, respectively. NH_3 adsorption peaks on Ag, Si and Al sites are located at 1020, 1231 and 1346 cm^{-1}, respectively, which are close to the respective experimental values, while the band of NH_3 adsorption on Fe sites is at 1164 cm^{-1}, which is higher 18 cm^{-1} than the experimental one. The simulated FTIR spectrum shows that NH_4^+ adsorption peaks on Brønsted acid site of Ag are located at 1650 and 1728 cm^{-1} (Fig. S6), which are close to the experimental values in Ag/Al_2O_3 (1652 cm^{-1}) and Ag/bauxite (1737 cm^{-1}), respectively.

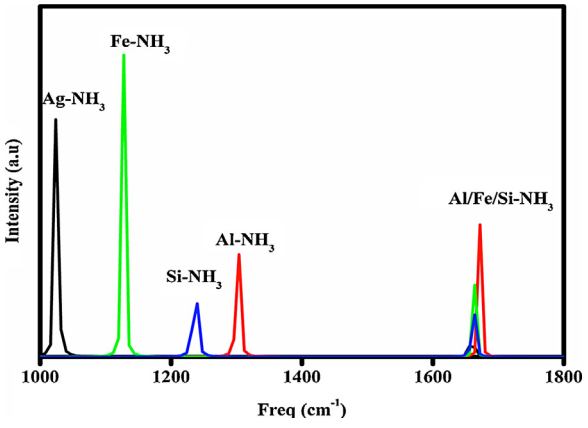

Fig. 7. The simulated vibration models of M–NH_3 (M = Ag, Fe, Si and Al).

4. Conclusions

A series of low-temperature and SO_2-tolerant Ag/bauxite catalysts were prepared. NO_x conversion of 3Ag/bauxite is much higher than that in $3Ag/Al_2O_3$ below 250 °C in SCR of NO_x. Moreover, 3Ag/bauxite exhibits stronger SO_2 tolerance and better regeneration ability than $3Ag/Al_2O_3$. FeO_x and Ag clusters are confirmed to be main active species in SCR of NO_x at low temperature, and the use of bauxite support increases Lewis acid sites in comparison with Al_2O_3, which is responsible for high activity of 3Ag/bauxite at low temperature. In summary, this study has demonstrated that Ag/bauxite is a promising alternative for Ag/Al_2O_3 in NH_3-SCR at low temperature, which provides a possibility for development of efficient low-temperature SCR catalysts.

Acknowledgements

This work was financially supported by 973 Program (2011CBA00502, 2013933202) and Major Project of Fujian Province (2013H0061, 2012H0049).

Appendix A. Supplementary data

Supplementary data associated with this article can be found, in the online version, at http://dx.doi.org/10.1016/j.apcatb.2014.10.080.

References

[1] (a) D.Y. Yoon, J.H. Park, H.C. Kang, P.S. Kim, I.S. Nam, G.K. Yeo, J.K. Kil, M.S. Cha, Appl. Catal., B: Environ. 101 (2011) 275–282;
(b) W. Fu, X.H. Li, H.L. Bao, K.X. Wang, X. Wei, Y.Y. Cai, J.S. Chen, Sci. Rep. 3 (2013) 2349;
(c) Z. Chen, X. Wang, R. Wang, ChemPlusChem 79 (2014) 1167–1175.
[2] (a) K. Paredis, L.K. Ono, F. Behafarid, Z. Zhang, J.C. Yang, A.I. Frenkel, B.R. Cuenya, J. Am. Chem. Soc. 133 (2011) 13455–13464;
(b) U. Deka, I. Lezcano-Gonzalez, B.M. Weckhuysen, A.M. Beale, ACS Catal. 3 (2013) 413–427;
(c) W. Shan, F. Liu, H. He, X. Shi, C. Zhang, Appl. Catal., B: Environ. 115–116 (2012) 100–106;
(d) L. Li, P. Wu, Q. Yu, G. Wu, N. Guan, Appl. Catal., B: Environ. 94 (2010) 254–262.
[3] (a) S. Fogel, D.E. Doronkin, P. Gabrielsson, S. Dahl, Appl. Catal., B: Environ. 125 (2012) 457–464;

(b) H. Chang, X. Chen, J. Li, L. Ma, C. Wang, C. Liu, J.W. Schwank, J. Hao, Environ.Sci. Technol. 47 (2013) 5294–5301;
(c) P.S. Kim, M.K. Kim, B.K. Cho, I.S. Nam, S.H. Oh, J. Catal. 301 (2013) 65–76;
(d) R.P. Vélez, I. Ellmers, H. Huang, U. Bentrup, V. Schünemann, W. Grünert, A. Brückner, J. Catal. 316 (2014) 103–111.
[4] (a) P. Forzatti, I. Nova, E. Tronconi, Angew. Chem. Int. Ed. 48 (2009) 8366–8368;
(b) A. Grossale, I. Nova, E. Tronconi, D. Chatterjee, W. Weibel, J. Catal. 256 (2008) 312–322;
(c) J. Shibata, K. Shimizu, Y. Takada, A. Shichi, H. Yoshida, S. Satokaw, A. Satsuma, T. Hattori, J. Catal. 227 (2004) 367–374.
[5] (a) S. Yang, C. Wang, L. Ma, Y. Peng, Z. Qu, N. Yan, J. Chen, H. Chang, J. Li, Catal. Sci. Technol. 3 (2013) 161–168;
(b) Y. Wan, W. Zhao, Y. Tang, L. Li, H. Wang, Y. Cui, J. Gu, Y. Li, J. Shi, Appl. Catal., B: Environ. 148–149 (2014) 114–122;
(c) Y. Peng, R. Qu, X. Zhang, J. Li, Chem. Commun. 49 (2013) 6215–6217.
[6] (a) D.E. Doronkina, T.S. Khan, T. Bligaard, S. Fogel, P. Gabrielssonand, S. Dahl, Appl.Catal. B: Environ. 117–118 (2012) 49–58;
(b) M.K. Kim, P.S. Kim, J.H. Baik, I.S. Nam, B.K. Cho, S.H. Oh, Appl. Catal., B: Environ. 105 (2011) 1–14;
(c) H. He, Y. Wang, Q. Ma, J. Ma, B. Chu, D. Ji, G. Tang, C. Liu, H. Zhang, J. Hao, Sci. Rep. 4 (2014) 4172.
[7] (a) U. Kamolphop, S.F.R. Taylor, J.P. Breen, R. Burch, J.J. Delgado, S. Chansai, C. Hardacre, S. Hengrasmee, S.L. James, ACS Catal. 1 (2011) 1257–1262;
(b) S. Tamm, S. Fogel, P. Gabrielsson, M. Skoglundh, L. Olsson, Appl. Catal., B: Environ. 136–137 (2013) 168–176;
(c) K. Shimizu, A. Satsuma, J. Phys. Chem. C 111 (2007) 2259–2264.
[8] J. Shibata, K. Shimizu, S. Satokawa, A. Satsuma, T. Hattori, Phys. Chem. Chem. Phys. 5 (2003) 2154–2160.
[9] D.E. Doronkin, S. Fogel, P. Gabrielsson, J.D. Grunwaldt, S. Dahl, Appl. Catal., B: Environ. 148–149 (2014) 62–69.
[10] P.M. More, N. Jagtap, A.B. Kulal, M.K. Dongare, S.B. Umbarkar, Appl. Catal., B: Environ. 144 (2014) 408–415.
[11] L. Valanidou, C. Theologides, A.A. Zorpas, P.G. Savva, C.N. Costa, Appl. Catal., B: Environ. 107 (2011) 164–176.
[12] N. Jagtap, S.B. Umbarkar, P. Miquel, P. Granger, M.K. Dongare, Appl. Catal., B: Environ. 90 (2009) 416–425.
[13] X. Wang, Z. Chen, Y. Luo, L. Jiang, R. Wang, Sci. Rep. 3 (2013) 1559.
[14] (a) K. Shimizu, A. Satsuma, Phys. Chem. Chem. Phys. 8 (2006) 2677–2695;
(b) M. Colombo, I. Nova, E. Tronconi, Appl. Catal., B: Environ. 111–112 (2012) 433–444.
[15] (a) D. Zhang, L. Zhang, L. Shi, C. Fang, H. Li, R. Gao, L. Huang, J. Zhang, Nanoscale 5 (2013) 1127–1136;
(b) Y. Shen, S. Zhu, Catal. Sci. Technol. 2 (2012) 1806–1810;
(c) C. Fang, D. Zhang, L. Shi, R. Gao, H. Li, L. Ye, J. Zhang, Catal. Sci. Technol. 3 (2013) 803–811.
[16] Y. Peng, K. Li, J. Li, Appl. Catal., B: Environ. 140–141 (2013) 483–492.
[17] (a) X. Yang, B. Zhao, Y. Zhuo, Y. Gao, C. Chen, X. Xu, Environ. Sci. Technol. 45 (2011) 1147–1151;
(b) L. Chen, J. Li, M. Ge, Environ. Sci. Technol. 44 (2010) 9590–9596.